Reflection tomography: vees in midpoint-offset space

Marta Jo Woodward

ABSTRACT

In reflection seismic experiments, localized velocity anomalies cast shadows on underlying reflectors—creating vee-shaped time-shift patterns in midpoint-offset space. Ray-theoretic, tomographic inversion of reflection seismic data for small velocity anomalies typically consists in the four-step identification of these patterns. A background velocity model is assumed; vees for point velocity anomalies at all midpoints are found by ray-tracing through the model; anomalous traveltimes are determined by picking crosscorrelation peaks, and the picked time shifts are backprojected into midpoint-depth space through integration over all possible vees on the midpoint-offset plane. This paper proposes two modifications to this four-step scheme. First, the reconstruction of small velocity anomalies is reformulated as an optimization problem. By shifting traces underlying precalculated vee-patterns up and down in time to maximize a semblance objective function, the algorithm estimates traveltime and velocity anomalies simultaneously—without intermediate picking. Second, wave effects noted through comparison of equivalent wave and ray-theoretic data sets are incorporated into the algorithm through modification of the ray-trace derived vee-patterns. Smearing the vees in midpoint and damping them in offset yielded improved inversion results for wave-theoretic data.

INTRODUCTION

In reflection seismic experiments, localized velocity anomalies cast shadows on underlying reflectors—creating anomalous time-shift patterns on expected arrival horizons in midpoint-offset space (Kjartansson, 1979; Ottolini and Rocca, 1982; Fulton and Darr, 1984; Claerbout, 1985). Figure 1 shows ray-theoretic shadows on horizontal and dipping planar reflectors, generated by point-anomalies in a constant velocity background field. The vee-shaped patterns open and close as the distances between the anomalous points and the reflecting surfaces increase and decrease. More complicated vees may be calculated or ray-traced through more complicated background velocity models for more complicated reflector structures.

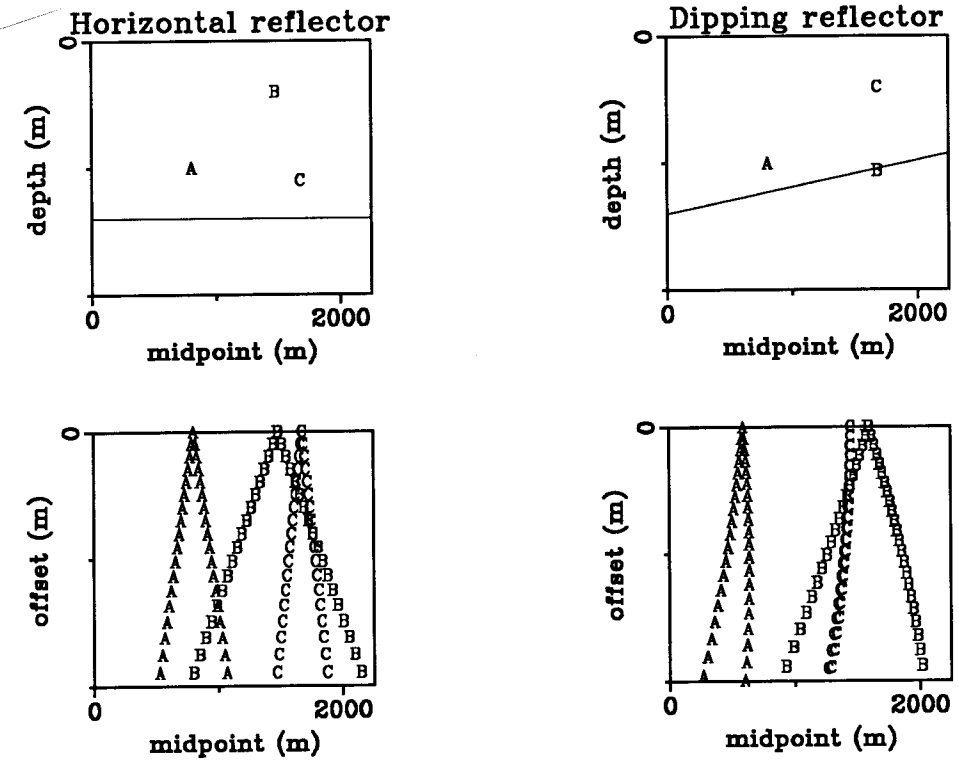

FIG. 1. The upper plots show point velocity anomalies (A, B and C) in a constant velocity background field. The lower plots show the ray-theoretic shadows cast by the anomalies on underlying horizontal and dipping reflectors. The shadows appear as traveltime perturbations in midpoint-offset space.

Ray-theoretic, tomographic inversion of reflection seismic data for small velocity anomalies typically consists in the four-step identification of these vee-shaped shadows in midpoint-offset space. A background velocity model is assumed; vees for point velocity anomalies at all midpoints and depths are calculated or ray-traced through the model; anomalous traveltimes are picked by crosscorrelating traces on normal moveout corrected common midpoint gathers; and, finally, the picked time shifts are integrated over all possible vees on the midpoint-offset plane (Kjartansson, 1979). This last, backprojection step corresponds to a generalized inverse Radon transformation from data (midpoint-offset) space to physical (midpoint-depth) space; a rho filter must be applied to complete the inversion (Fawcett and Clayton, 1984).

This paper proposes two modifications to the four-step scheme described above. The first is a reformulation of tomographic reconstruction as an optimization problem. By shifting traces underlying precalculated vee-patterns up and down in time to maximize a semblance objective function, the algorithm estimates traveltime and velocity anomalies simultaneously—without intermediate picking (following Ronen and Claerbout, 1985). The second modification is an attempt to design vee-patterns for wave-theoretic tomography. Two data sets are examined for a single reflection seismic experiment. One is wave-theoretically correct, generated by a wave-equation modeling program (Elastic2d, courtesy of Peter Mora); the other is the straight-ray equivalent of the former. Differences between the two data sets are noted and used to adjust ray-theoretic vee-patterns for wave-theoretic data.

REFLECTION SEISMIC EXPERIMENT

Figure 2a shows the velocity model used to generate the reflection seismic data sets considered in this paper. Five anomalous low velocity regions are embedded in a constant velocity medium overlying a horizontal, planar reflector at 625 m. From left to right across the page: the average velocities of the squares are 76, 83, 76, 83 and 89 percent of the background field (2100 m/s); the widths of the squares are .3, .6, .2, .6, and 1.2 times the dominant source wavelength of the experiment (84 m). The anomalous regions are tapered from higher to lower velocities from exterior to interior, size permitting. They are small for the purposes of minimizing raybending and of testing the resolution of the method.

Figure 2b illustrates the wave-theoretic data set created by wave-equation modeling a reflection seismic experiment over the given velocity field. A zero-offset section is shown (windowed in time around the reflector horizon), along with a time slice through the normal moveout flattened reflection in midpoint-offset space. The trace spacing and near half-offset are both 12.5 m; the source wavelet's dominant frequency is 25 Hz. The ray-theoretic equivalent of Figure 2b is shown in Figure 2c. Constructed by shifting traces with straight ray-trace derived time delays, the data set exactly fits the infinite frequency, straight ray assumptions of ray-theoretic tomography.

There are three major differences between the wave-theoretic and straight-ray-theoretic data sets. The first is the contamination of the former with hyperbolic artifacts—generated by reflections off the anomalous velocity zones. Prominent, backscattered, diffraction hyperbolas slice through the reflector in Figure 2b, disguising the vee-patterns on the midpoint-offset plane. This feature makes picking traveltime anomalies through crosscorrelation of traces on common midpoint gathers impossible. Hyperbolic events also originate on the reflector itself—appearing at the edges of the anomaly-induced time sags on the zero-offset section. They correspond to the reflection of energy scattered downwards by the square velocity anomalies.

The second difference between the data sets is the considerable broadening of the vee-patterns on the wave-theoretic time-slice panel. This phenomenon results from the interaction of the bandlimited source wavefield with the anomalous velocity regions. Since the first half-wavelength of any source-receiver event is influenced by an elliptical region surrounding the intervening straight-ray path (in a homogeneous medium), an anomalous velocity region influences more source-receiver pairs than predicted by tracing rays (Hagedoorn, 1957; Woodward, 1986). Figure 3 shows overlapping elliptical regions calculated for two midpoints separated by 125 m; the dominant source wavelength and reflector depth correspond to those of the experiment described above. The square anomaly is 50 m on a side. While ray theory predicts detection of the anomaly only at the midpoint on the left, wave theory implies its detection at the midpoint on the right.

Finally, the time shifts on the wave-equation data set are smaller than those on the ideal, ray-theoretic equivalent. Because the anomalous zones are on the order of a wavelength or less in size, they are generally smaller than the Fresnel zone of the source wavefield at their depth—and only weakly detected. This point is clarified through comparison of the time shifts below the second and fourth anomalous velocity zones. While the squares are of the same width and magnitude, their different depths imply different effective Fresnel zones. The Fresnel zone of the source wavefield is larger at the deeper, second anomaly—and the latter's related time shift is smaller. This phenomenon is known as wavefront healing.

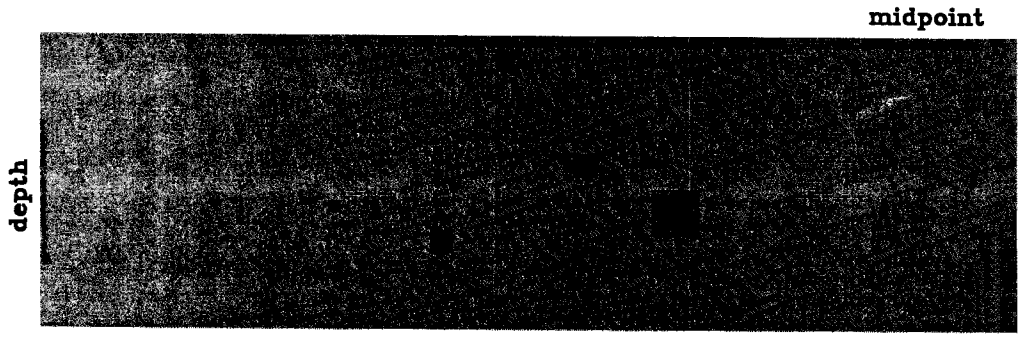

(a). Velocity model

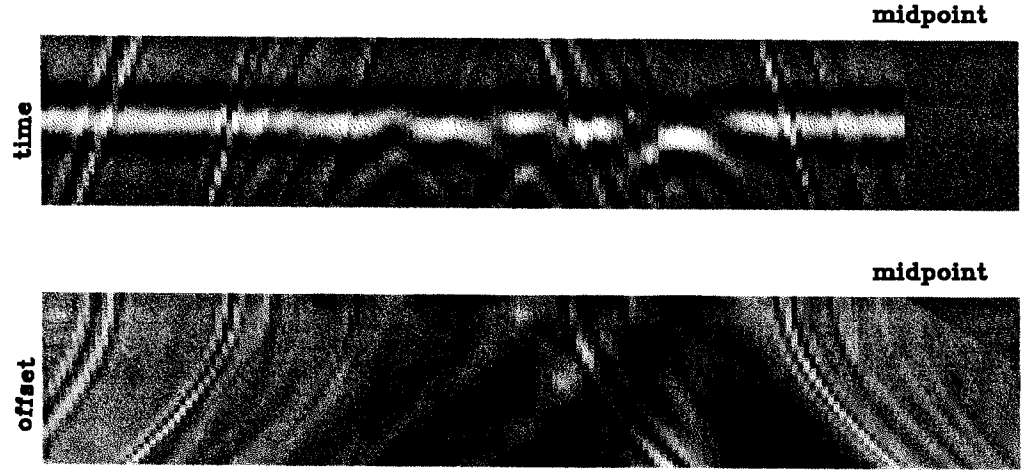

(b). Wave–theoretic data set

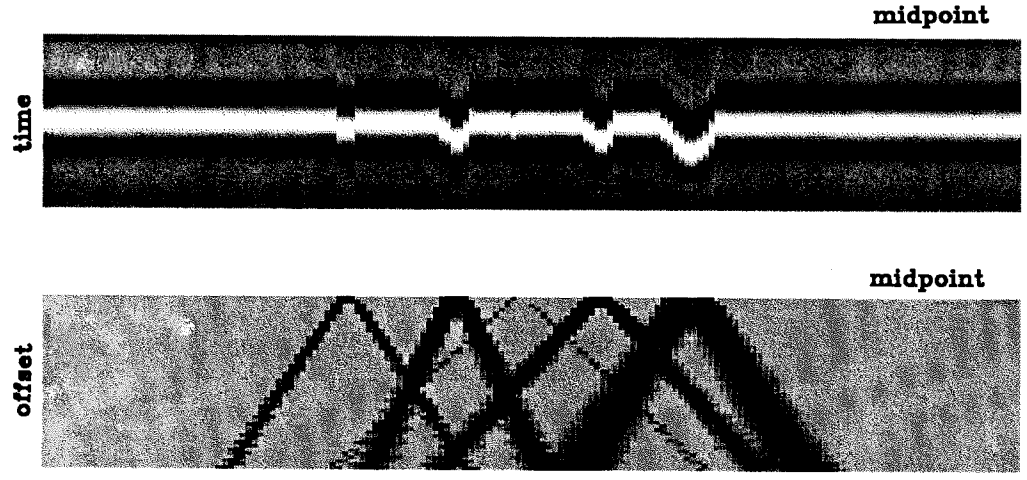

(c). Ray–theoretic data set

FIG. 2. A reflection seismic experiment. (a). The velocity model in midpoint-depth. (b). The wave-theoretic data set: a windowed zero-offset section in midpoint-time, and a time slice through the normal moveout corrected reflector in midpoint-offset. (c). The ray-theoretic data set: plots as described in (b).

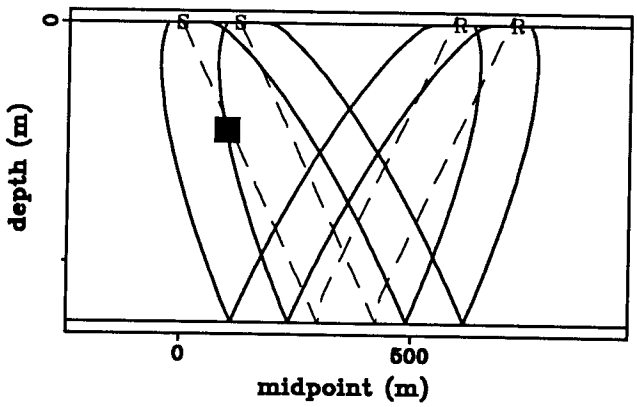

FIG. 3. Ray-paths connecting source-receiver pairs for two neighboring midpoints are shown as dashed lines. The elliptical regions influencing the first half-wavelength of corresponding bandlimited source-receiver events are shown as heavy solid lines. Ray theory predicts detection of the square anomaly only at the midpoint on the left; wave theory predicts its detection at both midpoints.

INVERSION FOR VELOCITY ANOMALIES

Ray-theoretic vees

The first step in the inversion of a reflection seismic data set for small velocity anomalies is the determination of the vee-patterns—the association of a time-shift shadow in midpoint-offset space with each possible perturbation location in physical, velocity space. For this application the background field was discretized into 12.5 m by 12.5 m squares—constraining the possible perturbation locations to fifty discrete depths. Representative vee-patterns are shown in Figure 4: the upper plot shows the shadow cast in midpoint-offset space by an anomaly at the surface of the model; the lower plot shows the shadow for an anomaly halfway between the surface and the reflector. In both cases, the apex of the vee points to the position of the velocity anomaly on the midpoint axis. The intensity of the vees at each midpoint-offset position is proportional to the path length travelled by the corresponding ray through the anomaly—and consequently to the time shift expected at that position. The fifty templates were normalized to a maximum relative time-shift value of one. Changing the magnitude of a velocity anomaly corresponds to multiplying a vee-pattern by a scale factor.

Model estimation by semblance optimization

Tomographic reconstruction of velocity perturbations typically inverts picked traveltime anomalies by backprojecting them over vees, normalized (as above) for path length. Because the strong diffraction events in Figure 2b preclude the successful picking of vee-pattern time-delays, an alternative method obviating picking was found. Ronen and Claerbout (1985) proposed statics estimation by stack-power maximization for data sets with similarly low signal-to-noise ratios. Taking normal moveout corrected data, they shifted traces corresponding to a single shot-receiver position up and down in time to maximize stack power over the section—estimating the statics model and the time shifts simultaneously. They iteratively swept across midpoint-offset space, imposing the best shift for each shot-receiver location as it was calculated. Since the statics problem is a special case of tomographic

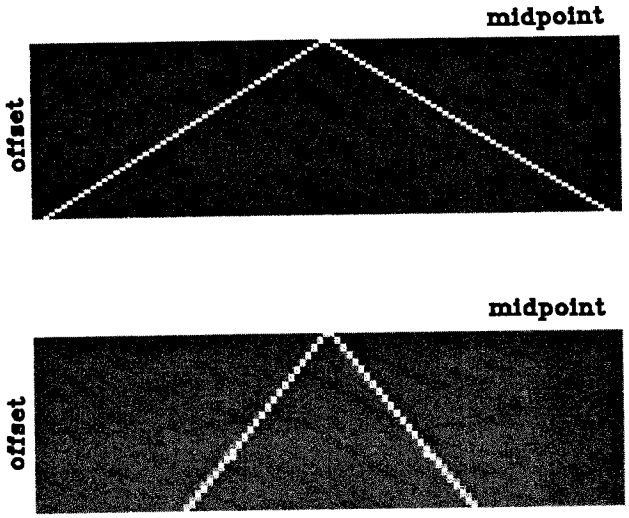

FIG. 4. Ray-theoretic vees: the upper pattern illustrates the time-shift shadow cast in midpoint-offset space by a single, square anomaly positioned at the surface of the model of Figure 2a; the lower pattern illustrates the shadow for a similar anomaly positioned half-way between the surface and the reflector.

inversion—constrained to the reconstruction of perturbations in the top-most layer of a velocity model—their method is readily extended to the full reflection tomographic problem. Instead of shifting only traces underlying vees corresponding to velocity anomalies at the surface (the upper plot in Figure 4), this application requires shifting traces underlying vees for anomalies at all depths. As in the statics problem, the tomographic model $\mathbf{m}$ is parameterized not in terms of anomalous velocities, but in terms of time shifts accruing to discrete anomaly positions—i.e., as weights applied to vee-patterns. For this exercise there were 3200 model parameters—corresponding to vee-patterns for 50 possible depths positioned at 64 possible midpoints.

Perhaps because of the increase in the number of model parameters in going from the statics problem to the full tomography problem, two changes had to be made to the statics optimization algorithm before it would work for the tomographic case. First, the objective function $Q(\mathbf{m})$ was altered from stack power. Both a semblance-over-offset function (used by Toldi, 1985, for his optimization-theory formulation of velocity analysis):

$$Q(\mathbf{m}) = \sum_i \sum_j \frac{\left(\sum_k d(t_i + \Delta t_{kj}(\mathbf{m}), h_k, y_j)\right)^2}{\sum_k \left(d(t_i + \Delta t_{kj}(\mathbf{m}), h_k, y_j)\right)^2} \tag{1}$$

and a semblance-over-reflector function (suggested by Stew Levin):

$$Q(\mathbf{m}) = \sum_i \frac{\left(\sum_j \sum_k d(t_i + \Delta t_{kj}(\mathbf{m}), h_k, y_j)\right)^2}{\sum_j \sum_k \left(d(t_i + \Delta t_{kj}(\mathbf{m}), h_k, y_j)\right)^2} \tag{2}$$

were tested. The variables t, y, and h refer to time, midpoint and offset in a data set, d—normal moveout corrected according to the background velocity field. The term $\Delta t_{kj}(\mathbf{m})$ describes the time shifts at h_k and y_j corresponding to an anomaly model $\mathbf{m}$. While the two objective functions were not compared rigorously, the semblance-over-reflector formula seemed to produce faster convergence.

Second, the search scheme was modified. Instead of imposing objective-function maximizing shifts as they were calculated at each location, a combination of the steepest-ascent and

conjugate-gradient methods was used (Gill et al, 1981). The gradient of the objective function with respect to the model parameters was calculated at each iteration by finite difference: at each midpoint position, vees corresponding to each depth were sequentially laid over the midpoint-offset plane; the underlying traces were shifted in time according to the magnitude of the vee at their position; the change in the semblance-over-reflector function was interpreted as $\partial Q/\partial m$ (m describing the vee-pattern being applied). Time-shifts were imposed on the data as steps in the gradient direction—or in a weighted combination of the gradient direction and the previous directions.

Ray-theoretic data set: ray-theoretic vees

The result of applying the inversion method described above to the ray-theoretic data set is shown in Figure 5. From top to bottom, the plots show: the zero-offset section after fourteen iterations (where convergence stopped, having increased the objective function by 33%); a time slice through the data set at the same time as in Figure 2c; the total time shifts applied in midpoint-offset space, and the inversion result produced by backprojecting these time shifts into midpoint-depth space. The method has done a good job at both defining the velocity anomalies of Figure 2a, and at removing the vee-shaped time sags in midpoint-offset space. Finite-aperture induced artifacts are apparent as diagonal smears across the inversion; the prominent sidelobes should be removed through application of a derivative-like rho filter (Fawcett and Clayton, 1984).

Wave-theoretic data set: ray-theoretic vees

The result of applying the inversion method to the wave-theoretic data set is shown in Figure 6, the plots paralleling those of Figure 5. For this case, convergence stopped at the seventeenth iteration, after a 21% increase in the objective function. While the method has succeeded in removing the vee-shaped traveltime anomalies, it has done a poor job of defining the velocity perturbations of Figure 2a. This failure is an expected result, given the large differences between the ideal, ray-theoretic data set and its wave-theoretic equivalent.

Wave-theoretic vees

To improve the tomographic inversion of the wave-theoretic data set, the ray-theoretic vees were modified according to differences noted between wave and ray-theoretic data. First, they were altered to reflect Fresnel zone phenomena. The source field for the reflection seismic experiment considered in this paper was a spherical wave; the larger the angle subtended by an anomaly along an expanding spherical wave, the closer its resultant time shift will be to its ray-theoretic time shift. As a consequence of this reasoning, the magnitudes along the ray-theoretic vees were multiplied by the ratio of the anomaly cross-section to the Fresnel zone of the expanding source wave, as measured at their intersection. (Actually this seemed to damp far offsets drastically; at the suggestion of John Etgen the factor was replaced by its square root.)

Second, the ray-theoretic vees were broadened. For each offset on each vee, the dimensions of the elliptical region influencing the first half-wavelength of a source-receiver event were calculated. The vees were then linearly tapered along midpoint from a ray-theoretic high point (corresponding to that midpoint position where the source-receiver ray intersected the anomaly), out to a midpoint with an ellipse just grazing the anomaly.

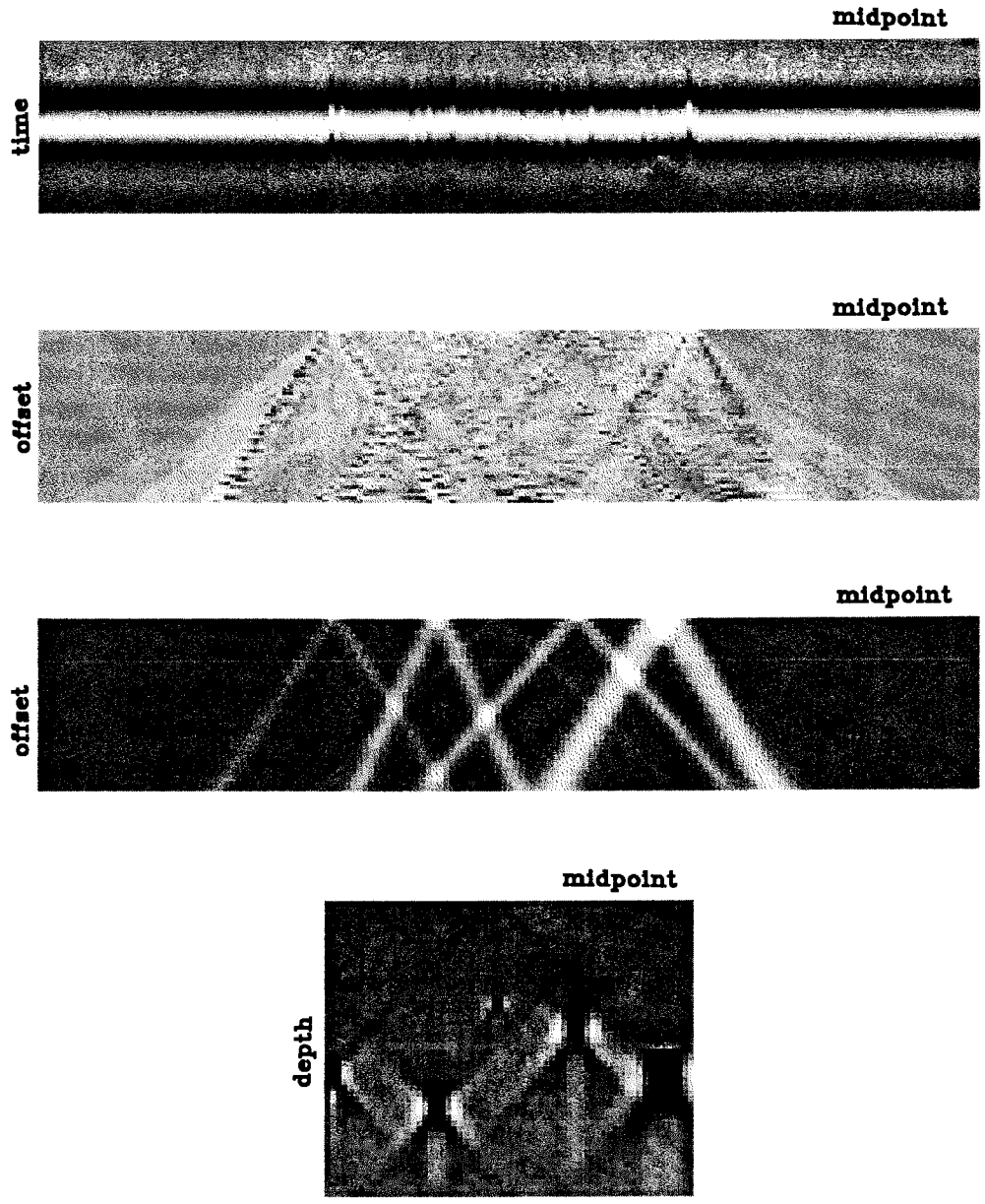

FIG. 5. Ray-theoretic data set inverted for velocity anomalies using ray-theoretic vees. From top to bottom the plots show: a zero-offset section; a time-slice panel; the time-shift corrections applied by the inversion; the backprojection of the applied time shifts to midpoint-depth space.

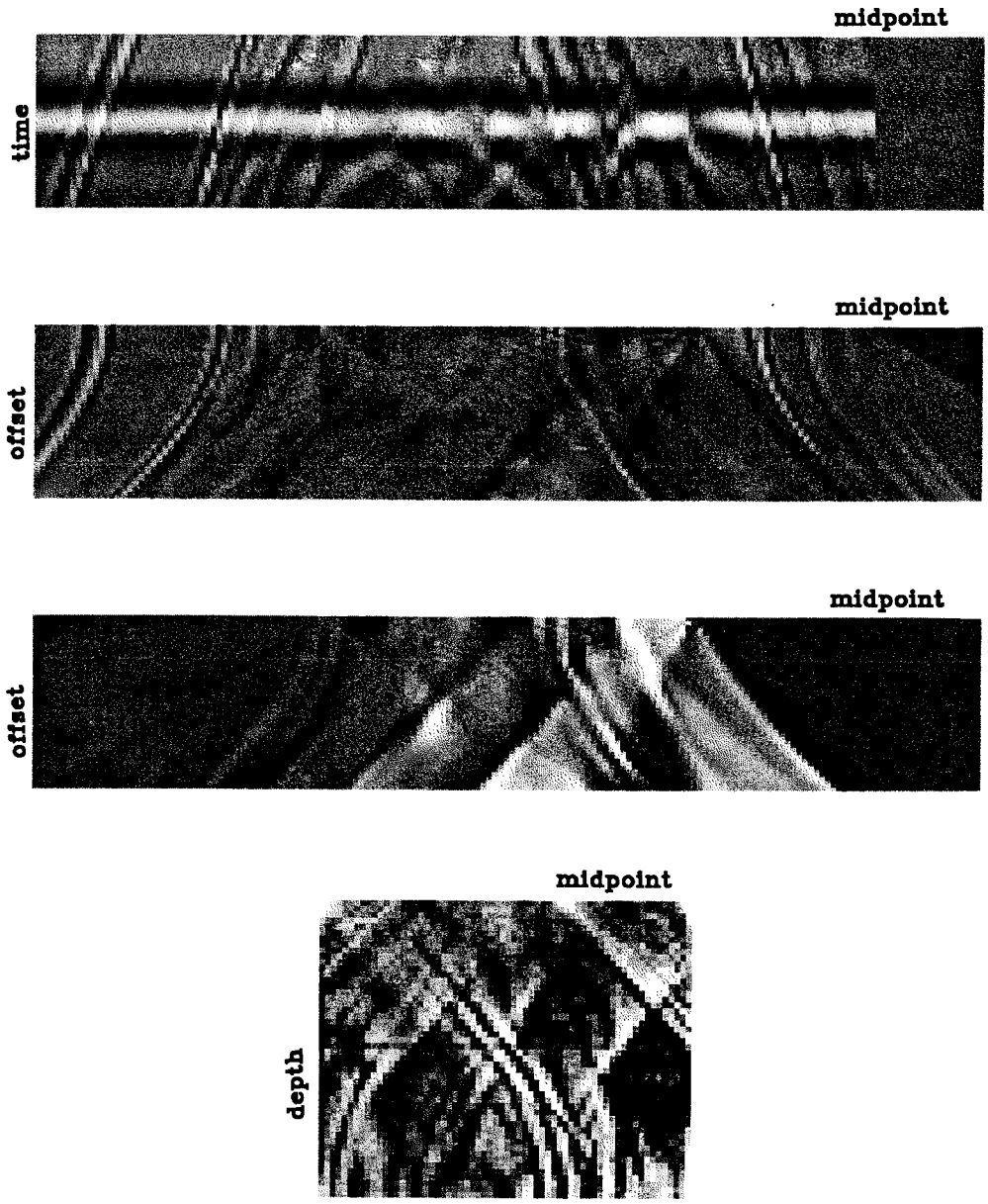

FIG. 6. Wave-theoretic data set inverted for velocity anomalies using ray-theoretic vees. From top to bottom the plots show: a zero-offset section; a time-slice panel; the time-shift corrections applied by the inversion; the backprojection of the applied time shifts to midpoint-depth space.

Figure 7 illustrates two pseudo-wave-theoretic vees created in this manner. As in Figure 4, the upper plot shows the wave-theoretic shadow cast in midpoint-offset space by an anomaly at the surface of the model; the lower plot shows the shadow for an anomaly half-way between the surface and the reflector.

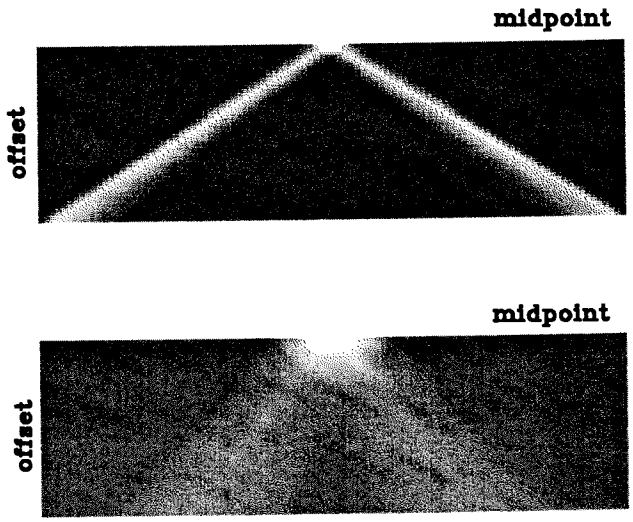

FIG. 7. Wave-theoretic vees: the upper pattern illustrates the time-shift shadow cast in midpoint-offset space by a single, square anomaly positioned at the surface of the model of Figure 2a; the lower pattern illustrates the shadow for a similar anomaly positioned half-way between the surface and the reflector.

Wave-theoretic data set: wave-theoretic vees

The result derived through application of the wave-theoretic vees to the wave-theoretic data set is shown in Figure 8. The plots correspond to those of Figures 5 and 6. For this case, convergence stopped after twenty-two iterations, with a 13% increase in the objective function. The wave-theoretic vees have done a better job of inverting the data set for small velocity perturbations than their ray-theoretic counterparts. The largest (1.2λ) anomaly is resolved very well; the ($.6\lambda$) anomaly immediately to its left is resolved moderately well—though shifted up slightly due to its interaction with its larger neighbor. The deeper ($.6\lambda$) anomaly is clearly indicated; the remaining two are questionably apparent. The vees corresponding to the deepest anomalies do not seem to fit the data well, having produced a ridge and then a relatively featureless zone in the bottom quarter of the inversion. The other artifacts are similar to those of Figure 5—aperture-induced smears diagonally crossing the picture. Again a rho filter should be applied to the result.

CONCLUSIONS

Successful tomographic reconstruction of small velocity anomalies depends on the correct identification of anomalous traveltimes. For noisy data sets, the independent determination of anomaly-induced time shifts may be difficult or impossible. The formulation of tomography as an optimization problem solves the picking problem by estimating traveltime and velocity anomalies simultaneously: time shifts are constrained to agree with a model.

Application of ray-theoretic tomography to reflection seismic data sets fails when velocity perturbations are on the order of the dominant source wavelength—when wave effects dominate ray theory. Wave effects may be incorporated into ray-theoretic tomography through modification of the precalculated vee-patterns describing the track of an

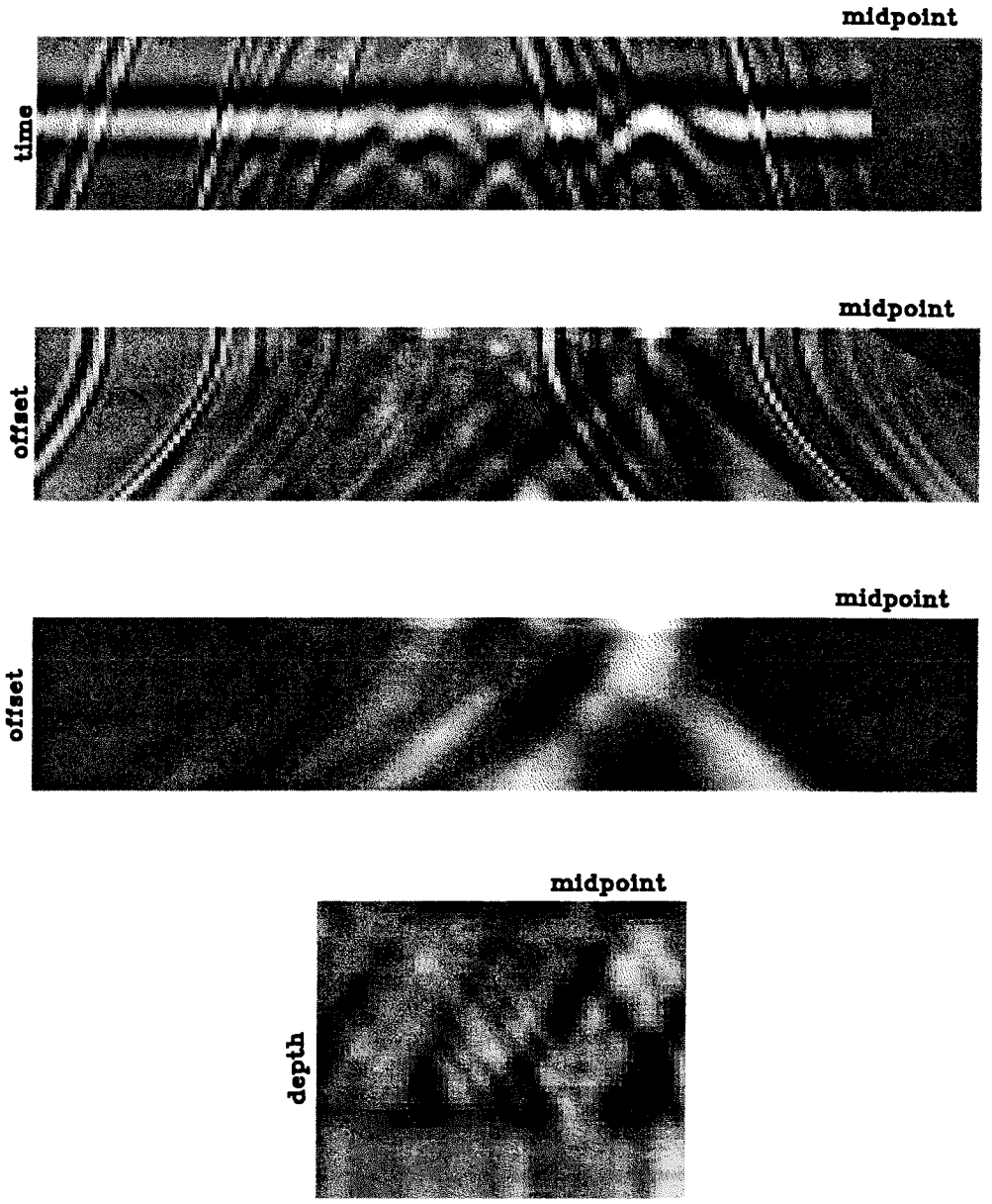

FIG. 8. Wave-theoretic data set inverted for velocity anomalies using wave-theoretic vees. From top to bottom the plots show: a zero-offset section; a time-slice panel; the time-shift corrections applied by the inversion; the backprojection of the applied time shifts to midpoint-depth space.

anomaly's shadow across midpoint-offset space. In this study, smearing vee-patterns in midpoint and damping them in offset yielded good resolution of anomalies on the order of a half-wavelength. These modifications were empirically determined and a more reasoned approach to their design needs to be developed.

ACKNOWLEDGEMENTS

John Etgen, Stew Levin, Fabio Rocca, Chuck Sword and Jos van Trier must be acknowledged for many helpful consultations. Steve Cole and Joe Dellinger also deserve thanks for creating the grey-scale plotting program used for most of this paper's figures.

REFERENCES

Claerbout, J.F., 1985, Imaging the earth's interior: Blackwell Scientific Publications.

Fawcett, J.A. and Clayton, R.W., 1984, Tomographic reconstruction of velocity anomalies: Bulletin of the Seismological Society of America, vol. 74, no. 6, p. 2201-2219.

Fulton, T.K. and Darr, K.M., Offset Panel, 1984: Geophysics, vol. 49, no. 8, p. 1140-1152.

Hagedoorn, J.G., 1954, A process of seismic reflection interpretation: Geophysical Prospecting, vol. 2, p. 85-127.

Gill, P.E., Murray, W., and Wright, M.H., 1981, Practical optimization: Academic Press Inc.

Kjartansson, E., 1979, Attenuation of seismic waves in rocks and applications in energy exploration, Stanford Ph.D. thesis.

Ottolini, R. and Rocca, F., 1982, Direct observation of lateral velocity anomalies in field data: SEP-32, p. 15-23.

Ronen, J., and Claerbout, J.F., 1985, Surface-consistent residual statics estimation by stack-power maximization: Geophysics, vol. 50, no. 12, p. 2759-2767.

Toldi, J.L., 1985, Velocity analysis without picking, Ph.D. thesis, Stanford University.

Woodward, M.J., 1986, Iterative tomography: error projection along ellipses and lines: SEP-48, p. 35-43.